The Astrophysical Journal, 864:102 (7pp), 2018 September 10 https://doi.org/10.3847/1538-4357/aad909

Chemical Diagnostics of the Massive Star Cluster-forming Cloud G33.92+0.11. II. HDCS and DCN

Young Chol Minh[1], Hauyu Baobab Liu[2], Roberto Galvań-Madrid[3], Dipen Sahu[4], Jinhua He[5,6,7], and Tatsuhiko Hasegawa[2]
[1] Korea Astronomy and Space Science Institute, 776 Daedeok-daero, Yuseong, Daejeon 34055, Republic of Korea
[2] Institute of Astronomy and Astrophysics, Academia Sinica, P.O. Box 23-141, Taipei 10617, Taiwan
[3] Centro de Radioastronomía y Astrofísica, UNAM, A.P. 3-72, Xangari, Morelia 58089, Mexico
[4] Physical Research laboratory, Navrangpura, Ahmedabad, Gujarat 380009, India
[5] Key Laboratory for the Structure and Evolution of Celestial Objects, Yunnan Observatories, Chinese Academy of Sciences, 396 Yangfangwang, Guandu District, Kunming, 650216, People's Republic of China
[6] Chinese Academy of Sciences South America Center for Astronomy, China-Chile Joint Center for Astronomy, Camino El Observatorio #1515, Las Condes, Santiago, Chile
[7] Departamento de Astronomía, Universidad de Chile, Casilla 36-D, Santiago, Chile
Received 2018 May 30; revised 2018 August 7; accepted 2018 August 8; published 2018 September 5

Abstract

The central region of the massive star-forming cloud G33.92+0.11 was investigated with the emission from the deuterated species HDCS and DCN observed at sub-arcsecond angular resolution (∼0.″7) using ALMA. HDCS shows a distributed emission throughout the region, and its large relative abundance in the most recent star-forming region suggests that there still exists a significant amount of cold gas associated with the hot core region. A high degree of HDCS fractionation ($HDCS/H_2CS > 0.1$) was found in the north region between star-forming clumps where the cold dense pre-collapse gas may still exist. DCN appears to have a good correlation with the continuum emission. This species traces both cold and warm dense gas probably by typical cold deuterium fractionation reactions and also by the lukewarm fractionation reactions. Near the densest cores where massive stars have already formed and dust mantles are evaporating, the DCN/HDCS abundance ratio was found to be larger by a factor of a few than other positions. This may suggest that the DCN abundance has been increased through the lukewarm fractionation processes in the gas phase.

Key words: ISM: abundances – ISM: individual (G33.92+0.11) – ISM: molecules – radio lines: ISM

1. Introduction

High-mass star-forming regions contain diverse features associated with the formation of energetic massive stars; these form in groups/clusters and evolve rapidly (e.g., Zinnecker & Yorke 2007; Reipurth & Yan 2008). Consequently, these regions show extreme complexity due to the presence of sub-regions with largely different physical/chemical conditions. High-mass star formation is one of the major events that govern the overall evolution of galaxies, but their early-phase evolutionary features are still poorly constrained, both observationally and theoretically (e.g., Zinnecker & Yorke 2007; Tan et al. 2014). For these complicated regions, chemical diagnostics is a powerful and often unique tool for investigating the nature of the source deeply embedded within the very dense molecular cloud (e.g., for G33.92+0.11). In this paper, we diagnose a complicated massive star cluster-forming region G33.92+0.11 (Liu et al. 2015; Minh et al. 2016) using the deuterated species HDCS and DCN observed with a high angular resolution (∼0.″7) using ALMA.

Deuterium (D) fractionation, the abundance change of a deuterated molecule relative to its non-deuterated form, has been intensively investigated with various species toward interstellar molecular clouds since the first detection of DCN in space (Jefferts et al. 1973). The degree of fractionation is largely determined along the past trace of the temperature and density of the molecular cloud, and it is found to increase greatly in some sources compared to the cosmic D/H ratio ($\sim 10^{-5}$, Linsky et al. 1993; Oliveira et al. 2003). This increase is by a few orders of magnitude in cold ($T_{\rm kin} \sim 10$ K) dark clouds (e.g., Roueff & Gerin 2003; Ceccarelli et al. 2007; Herbst & van Dishoeck 2009). It occurs mainly because of the exothermicity of deuterium exchange reactions, led by the dissociative recombination reaction of H_2D^+, as well as the depletion of, for example, CO molecules in cold dense gas which destruct H_2D^+ (e.g., Caselli et al. 1999; Gerlich et al. 2002; Roberts et al. 2002; Bacmann et al. 2003; Willacy 2007; Roueff et al. 2007; Daniel et al. 2007; Emprechtinger et al. 2009). One of our observed species, HDCS, the singly deuterated H_2CS, is thought to be fractionated through this typical deuteration process in the cold gas phase even to a very high level (Minowa et al. 1997; Marcelino et al. 2005). However, such as the case for H_2CO (Roberts & Millar 2000; Roberts et al. 2002), this species may further be fractionated in the grain mantles.

Another observed species is DCN, the deuterated HCN, which shows a high degree of fractionation in warm gas (e.g., Lis et al. 2002; Ren et al. 2012; Zinchenko et al. 2012), including the coma of the Hale-Bopp comet (Meier et al. 1998). It seems clear for the community that gas-phase chemistry is the dominant process responsible of the production of DCN. Several works (Turner 2001; Roueff et al. 2007) indicated that DCN can be formed both at low and high temperatures, from H_2D^+ and CH_2D^+, respectively. What it is interesting about HCN is that unlike most molecules, for which the deuteration process in the gas-phase is not efficient at temperatures above 20 K, the formation of DCN is also possible by reactions which can be efficient up to temperatures above 70 K (i.e., $CH_3^+ + HD \rightarrow CH_2D^+ + H_2 + 654$ K, Roueff et al. 2013). The commonly found deuterated fraction levels of ∼0.001 are typically an order of magnitude lower than the deuteration of H_2CO and CH_3OH, whose deuterated species are formed on the surface of grain mantles. Roueff et al. (2007) models form

Table 1
Observed Molecular Transitions

Molecule	Transition	Rest Frequency[a] (GHz)	E_{up} (K)
HDCS	$7_{0,7} - 6_{0,6}$	216.66243	41.6
$H_2C^{34}S$	$7_{1,7} - 6_{1,6}$	232.75471	57.9
DCN	3−2	217.23863	20.9

Note.
[a] From the NIST database at http://www.nist.gov/pml/data/micro/index.cfm.

efficiently DCN at low temperature, but noted that the abundance suffers a strong increase with the temperature. Indeed, Gerner et al. (2015), in a sample of massive dense cores, observed that the DCN/HCN ratio peak at the hot core stage. Additionally, Busquet et al. (2017), interpreting observations of the protostellar shock L1157-B1, concluded that DCN is formed by gas chemistry preferentially in hot gas. At temperatures above 20 K, the reverse reaction of this reaction: $H_3^+ + HD \rightarrow H_2D^+ + H_2$ becomes important, and this enhances the production of DCN via $CH_3^+ + HD \rightarrow CH_2D^+ + H_2 + 654$ K (Roueff et al. 2013), as suggested by chemical models (e.g., Roueff et al. 2007, 2013) and also by observations of the Orion Bar (Leurini et al. 2006; Parise et al. 2009). The high deuteration observed toward warm dense gas is, however, believed to result mainly from the evaporation of the grain mantle material either processed on the grain surface or accreted before the temperature increases (e.g., van Dishoeck et al. 1995; Rodgers & Millar 1996; Roberts & Millar 2000; Tiné et al. 2000; Aikawa et al. 2001; Osamura et al. 2004; Pillai et al. 2007; Fontani et al. 2011, 2015; Das et al. 2016; Belloche et al. 2016). The detection of multiply deuterated species with high abundance are especially believed to need grain surface reactions instead of forming in the gas phase (e.g., Loinard et al. 2000, 2001; Ceccarelli et al. 2001).

The observed source, G33.92+0.11, is a massive star cluster-forming region at a distance of 7.1 kpc, and it shows a nearly face-on projection (Fish et al. 2003; Liu et al. 2012). In a previous paper (Minh et al. 2016), we reported the observational properties of several molecules: the saturated hot core species, CH_3OH and CH_3CN; the turbulence-sensitive species, OCS, H_2S, and SO_2; and the shock tracer, SiO. These species display a large chemical diversity along the sub-clumps associated with star formation. The most prominent gas clumps are associated with the dust emission peaks A1, A2, A5, and A9. These numbers are from the dust continuum peaks identified in source A (central ∼1 pc area of the G33.92+0.11 cloud, Liu et al. 2015). We use this label to call the sub-clumps containing the continuum peak (Minh et al. 2016). Masses of these sub-clumps are about 100–300 $M_\odot$ (Watt & Mundy 1999; Liu et al. 2012). A1 and A2 are the most massive clumps in the observed region, which are strongly influenced by previous star formation activity, resulting in the UC H II region. This is the site embedding the probably first generation massive star-cluster. The most recent star formation is observed to be taking place in the A5 clump as described in Minh et al. (2016). Multiple SiO outflows have been found in association with A5, suggesting a new generation of stars that probably form as a cluster. We also believe that part of the chemical complexity of this region resulted from the accreting gas from the ambient clouds, especially in the northwestern part of A1 and the southern part of A2. The chemical complexity found in this region is thought to be largely due to the different chemical evolutionary timescales of the sub-clumps associated with massive star formation.

This work is focused on the deuteration of two interstellar molecules to investigate the early evolutionary phase of a complex massive star-forming region. We briefly summarize the ALMA observations made in Section 2. Section 3.1 includes the observed results for the molecular transitions from the deuterated species HDCS and DCN together with $H_2C^{34}S$. Section 3.2 explains the abundance derivation of observed molecules and total column density from dust continuum emission. Then, we discuss on the implications of our results for HDCS and DCN in Section 4, followed by a summary in Section 5.

2. Observations

Observations were made using the ALMA 12 m array on 2014 May 04. Table 1 lists the molecular transitions used for the analyses. The pointing and phase referencing center is (R.A., decl.)$_{J2000}$ = ($18^h52^m50^s.272$, $00°55'29''.604$). We used two 234.4 MHz wide spectral windows (channel spacing 61 kHz, ≈0.085 km s^{-1}) and two 1875.0 MHz wide spectral windows (channel spacing 488 kHz, ≈0.65 km s^{-1}), which tracked the velocity v_{lsr} = 107.6 km s^{-1} on our target source. We observed Titan, J1851+0035, and J1751+0939 for absolute flux, gain, and passband calibrations. Further observational details can be found in Liu et al. (2015). The resulting angular resolutions are about 0.″6–0.″8 (the *uv* sampling range was 13–430 kλ) in the observed frequencies. The 0.″6 is roughly 0.02 pc (∼4300 au) at a 7.1 kpc distance. The system temperatures were in range of 60–150 K and the spectral flux uncertainties of the observed lines were about 20–50 mK (1σ). As explained in Minh et al. (2016), we expect that this data will suffer some missing flux with emission scales ⩾8″, but we focus on more compact structures less affected by missing flux.

3. Results

3.1. Emission Distributions

Figure 1 shows the emission distribution of the observed species, HDCS ($7_{0,7}$–$6_{0,6}$), $H_2C^{34}S$ ($7_{1,7}$–$6_{1,6}$), and DCN (3−2), compared to the dust continuum emission of Liu et al. (2015) used a tracer of the total gas component. As explained in prior works and in the introduction (Liu et al. 2015; Minh et al. 2016), there exist several prominent sub-clumps in this source that show different chemical properties. In the upper left panel of Figure 1, we indicated four major sub-clumps, labeled as A1, A2, A5, and A9. The peak emission positions of the observed molecular emissions are shown in this panel. Since these positions do not coincide with each other, it was necessary to choose some compromised locations to compare their line profiles. The black crosses in this panel are the selected positions to take the line profiles for abundance comparison, as representative positions of each clump (A1, A2, A4, and A9). These positions are indicated with black circles by putting numbers 1 ∼ 6 in the 3 panels for molecular emissions of Figure 1.

HDCS and $H_2C^{34}S$ (upper right and lower left panels of Figure 1) show distributed emission throughout the region. Both species show a bright emission in the region associated

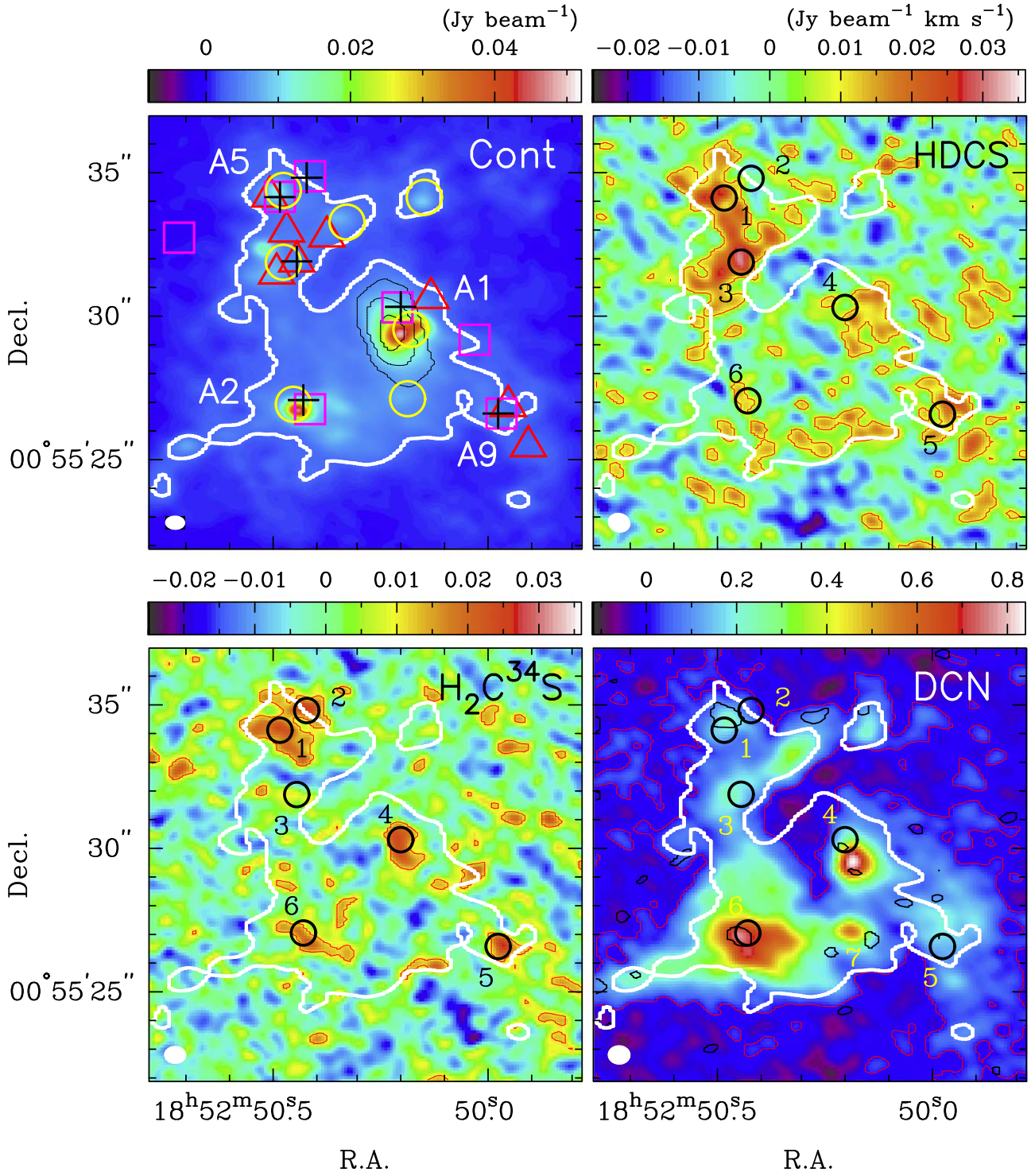

Figure 1. Integrated intensity maps of the continuum, HDCS $7_{0,7} - 6_{0,6}$, $H_2C^{34}S$ $7_{1,7} - 6_{1,6}$, and DCN 3−2 transitions as indicated in the top right of each panel. The continuum data is from Liu et al. (2015). Intensity scale of the false color image is shown as a bar at the top of each panel in units of Jy beam^{-1} for the continuum emission and Jy beam^{-1} km s^{-1} for the molecular lines. The white contour line included in each panel is the outline of the continuum emission strength of 3 mJy beam^{-1}. The black contour lines in the continuum panel are the H30α intensities with a scale of 0.5, 1, and 2 Jy beam^{-1} km s^{-1} (Minh et al. 2016). In this panel, we also show molecular emission peak positions in red triangles for HDCS, magenta squares for $H_2C^{34}S$, and yellow circles for DCN. Black crosses are the selected positions for line comparison, which are shown with black circles ($\sim$1″ in diameter) in molecular map panels. These circles are labeled from 1 to 6 to distinguish the positions. The red contours in the molecular map panels are for the 5σ uncertainty of each map. Synthesized beams are shown in the bottom-left corner of each panel.

with A5, which is where the latest star formation occurs energetically, as indicated by the existence of hot cores and SiO outflows (Minh et al. 2016). Especially, the HDCS emission is observed to be strong toward the region between A5 and the most massive A1 and A2 clumps, and no appreciable emission was found in this region from the molecules, such as ^{13}CS, hot core species, and sulfur-containing molecules, reported in Minh et al. (2016). This HDCS-enhanced region is a part of the "arm-c3," one of five molecular arms identified in this region by Liu et al. (2015) from the dust continuum emission distribution.

Although it is not clear whether this feature is actually a continuous gas clump, there seems to exist cold gas in this region unlike other dense molecular clumps (Y. C. Minh et al. 2018, in preparation).

DCN shows a good correlation with the dust emission in general, as previously noted by Liu et al. (2015). This emission is particularly very strong toward the A1 and A2 peaks, and is observed to be extended over the whole clumps. The expanding gas from the UC H II region (the black contours of the upper left panel of Figure 1) may have enhanced the density and temperature of this core. This elevated density and temperature seem to be the favorable condition to DCN formation. The A2 clump may also be interacting with the expanding UC H II region and with the incoming gas flow from the southern part, as suggested by the enhanced H_2S emission in this region (Minh et al. 2016). It is probably that the whole A2 clump is affected by shocks and the warm dense gas dominates in this clump.

3.2. Abundances

Figure 2 shows sample spectra obtained toward the black circle positions in Figure 1. These positions were selected roughly toward the peak emission position of the observed transitions to compare the abundances with each other. Spectra were obtained by averaging over the 1″ diameter circles in the figure. The 1″ diameter was roughly the half-power size of the identified cores in addition to considering the beam size. Some of them are weak in intensity, but they mostly show relatively simple profiles. The parameters of these lines were derived by Gaussian fitting of the line and listed in Table 2. The line velocities and widths of the spectra are roughly consistent to 108–109 km s^{-1} and 2–4 km s^{-1}, respectively, among the observed species. It may indicate that, in general, they are well associated in the region. However, some lines show multiple peaks—for example, the $H_2C^{34}S$ spectra of (1) and (6)—which results in larger linewidths than seen in the other lines. In any case, they were treated as a single line considering the weakness of the flux.

Table 3 lists the total column density ($N_{\rm column}$) derived from the integrated intensities listed in Table 2. We assumed an optically thin emission and Local Thermodynamic Equilibrium conditions using the following equation (cf. Irvine et al. 1987):

$$N_{\rm column} = \frac{2\pi\ \nu^2\ k}{h\ c^3 f_u\ A} \int T_R^*\ d\nu \qquad (1)$$

where ν is the line frequency, k is the Boltzmann constant, $\int T_R^*\ d\nu$ is the integrated brightness temperature of the line, h is the Planck constant, c is the velocity of light, f_u is the fractional population of the upper level of the line, and A is the Einstein A coefficient of the line. We applied a rotational temperature ($T_{\rm rot}$) range of 20–80 K to derive the fractional population (f_u) of the observed species. This temperature range covers the estimated temperature values by previous works (Liu et al. 2012; Minh et al. 2016). The major source of uncertainties in the column density calculations is the applied $T_{\rm rot}$ range. In the uncertainty calculation, we also included the observed spectral flux uncertainty in the 7th column of Table 3. The total uncertainties were added in quadrature and they are listed in the brackets after each column density value in Table 3. Since the observed lines were taken simultaneously in the same observation and have similar frequencies, we expect that a significant part of the calibration uncertainty will cancel out when deriving the abundance ratios between the observed values. One thing to note is that the energy levels of the observed transitions of HDCS and $H_2C^{34}S$ are very similar (Table 1), lessening the uncertainty resulted from the excitation difference between these species.

The H_2 column density in Table 3 was derived from the dust continuum emission at 1.3 mm (Liu et al. 2015). The emission strength of each position was averaged over the same area (1″) of the listed molecular emission. We applied the same parameters discussed in Section 4.1 of Liu et al. (2015) to calculate the total gas abundance from the observed continuum emission. Thus, $T_{\rm dust} = 30$ K was applied for the spectra positions 1, 4, and 6, and $T_{\rm dust} = 20$ K was used for the positions 2, 3, and 5 (Liu et al. 2015). The H_2CS abundances were estimated from the $H_2C^{34}S$ result using the ratio $CS/C^{34}S = 20$ (the isotope ratio is roughly in the range ∼20–22 for local interstellar medium, Wilson & Rood 1994; Chin et al. 1996; Hatchell et al. 1998). We derive the resulting abundance ratios $H_2CS/H_2 = \sim(1–2) \times 10^{-8}$ and $DCN/H_2 = \sim(1–3) \times 10^{-10}$ toward the selected positions (Table 3). The deuterium fractionation level of HDCS was found to be $\geqslant$0.1 toward the position 3, and about 0.01−0.03 toward other positions.

Both DCN and H_2CS have been widely observed toward various sources (e.g., Roberts et al. 2002; van der Tak et al. 2003; Parise et al. 2009; Ginard et al. 2012; Ren et al. 2012; López-Sepulcre et al. 2013; Gerner et al. 2015). Compared to previous results, our DCN abundance ($\sim(1–3) \times 10^{-10}$ relative to H_2) is pretty similar, but the H_2CS abundances ($\sim(1–2) \times 10^{-8}$) are higher by more than an order of magnitude to those obtained toward the regions associated with star formation. Except the chemical differences, if the observed emission is strong and well extended, such as that of DCN, the "beam-averaged" abundances will not change much along the observed beam sizes. On the other hand, if the emission is weak and very localized, such as the HDCS and $H_2C^{34}S$ emissions, the beam-averaged values should largely be dependent on the observed beam sizes, which could explain a part of the difference between the present and previous values.

4. Discussion

The massive star-forming region G33.92+0.11 shows a high degree of complexity as observed with various chemical tracers, such as hot core species and shock-related species in addition to general density tracers, such as CS or continuum emission (e.g., Minh et al. 2016). This may suggest that the associated dense sub-clumps experience different physical/chemical conditions due to the influence of the massive star formation activities. The chemistry in this region, which is believed to be far from equilibrium, may reflect the segregated evolutionary differences within a star-forming cloud that change over a relatively short timescale (∼10^3–10^4 years). Deuterated species, such as HDCS or DCN, could be a good tracer to distinguish physical/chemical properties of the region through the unique chemistry related to deuteration.

4.1. HDCS

As discussed by Minowa et al. (1997, Section 1), H_2CS is thought to be efficiently fractionated in cold gas by typical fractionation reactions, including H_2D^+. If the HDCS

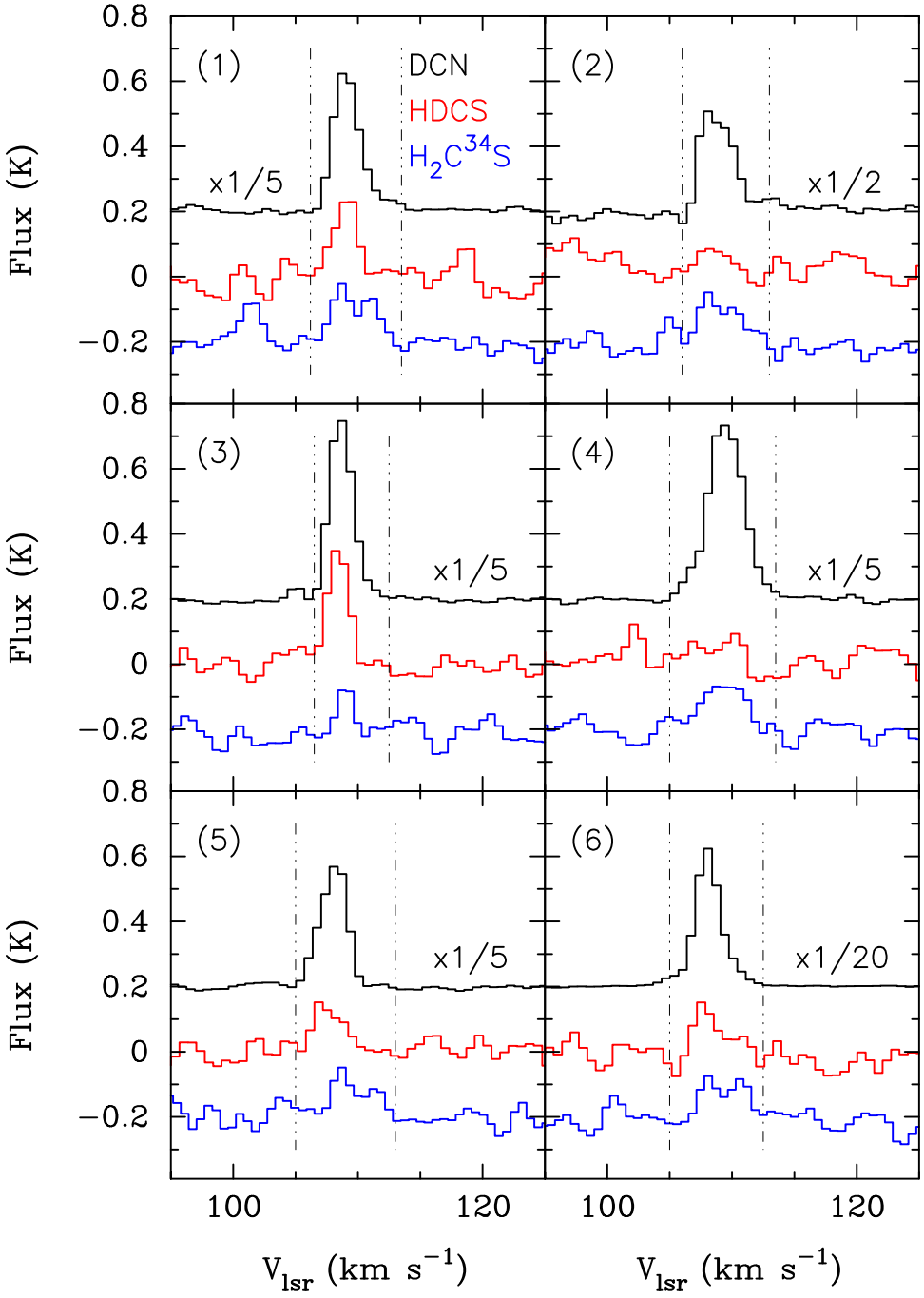

Figure 2. Spectra of DCN (3−2), HDCS ($7_{0,7}$ – $6_{0,6}$), and $H_2C^{34}S$ ($7_{1,7}$ – $6_{1,6}$) taken at the positions indicated with black circles (1″ in diameter) in Figure 1. The actual DCN spectrum has been reduced by a factor indicated in the spectrum. The dotted–dashed lines in each panel indicate the velocity range for deriving the total column densities (Section 3).

abundance is also enhanced by desorption from grains, we may see the enhancement of this species toward the A1 and A2 warm dense cores, which is not the case in this source. We found that the abundance ratio HDCS/H_2CS has an approximately 5–10 times larger value (≈0.12) in position 3 than in the other positions (Figure 2 and Table 3). Compared to the previous result, this value is lower but comparable to the high values found in the dark cloud B1 (Marcelino et al. 2005). On the other hand, the abundance ratios in the other positions are in the range of 0.01–0.03, similar to the dark cloud complex TMC-1 value (0.02, Minowa et al. 1997; Marcelino et al. 2005). According to the model of Marcelino et al. (2005), the degree of the H_2CS deuterium fractionation can largely be enhanced by including additional fractionation reactions of several ions, but it slightly changes if the density increases.

In the region associated with position 3, there seems to be a large abundance of cold dense gas, as revealed by the appreciable dust continuum emission and the lack of warm dense gas species, such as ^{13}CS (Minh et al. 2016; Y. C. Minh et al. 2018, in preparation). The large difference in the deuterium fractionation level even in cold clouds may result

Table 2
Line Parameters[a] of the Spectra in Figure 2

Pos.[b]	Mol.	v_{lsr} (km s^{-1})	T_{peak} (K)	Δv(HPW) (km s^{-1})	$\int T\,dv$[c] (K km s^{-1})	rms(1σ) (mK)
1	DCN	109.1	2.12	2.5	5.89	45
	HDCS	108.4	0.23	2.1	0.59	37
	$H_2C^{34}S$	109.6	0.18	4.2	0.57	24
2	DCN	109.0	0.61	2.5	1.98	34
	HDCS	108.5	0.09	2.6	0.25	35
	$H_2C^{34}S$	108.8	0.15	4.4	0.48	25
3	DCN	108.6	2.73	2.4	6.58	40
	HDCS	108.4	0.35	2.1	0.74	30
	$H_2C^{34}S$	109.0	0.12	1.1	0.17	35
4	DCN	109.5	2.67	3.4	9.82	32
	HDCS	108.6	0.09	3.3	0.29	24
	$H_2C^{34}S$	109.3	0.13	3.7	0.59	28
5	DCN	108.0	1.84	2.4	5.05	36
	HDCS	107.6	0.15	3.7	0.41	29
	$H_2C^{34}S$	109.3	0.15	4.2	0.48	28
6	DCN	108.1	8.48	2.4	22.2	32
	HDCS	107.9	0.15	2.3	0.37	35
	$H_2C^{34}S$	109.6	0.13	4.9	0.40	32

Notes.
[a] From Gaussian fittings.
[b] Positions shown in Figure 1 with circles (diameter = 1″).
[c] Total flux intensity integrated in the velocity range indicated in Figure 2.

from different abundance of free electrons, which is critical in destruction of ions necessary for further fractionation of H_2CS. The abundance ratios in other positions may indicate that the massive star-forming regions evolve rapidly and that a significant amount of cold gas still exists together with warm dense gas, resulting in a similar abundance ratio with TMC-1. Especially, the large abundance of HDCS in position 1, where a new generation of massive stars is forming as a group or cluster (Minh et al. 2016), may suggest that the massive star formation is occurring fast enough for the region to preserve together the pre-collapse phase cold dense gas.

4.2. DCN

The DCN emission was observed widespread over this massive star-forming region. It shows a relatively constant abundance of about (1–3) $\times$ 10^{-10} relative to H_2 in the observed regions (Table 3), which is similar to the values obtained for various other sources (a few $\times10^{-10}$–10^{-11}, e.g., Roberts et al. 2002; Parise et al. 2009; Ginard et al. 2012; Ren et al. 2012). The DCN emission show a good morphological correlation with the dust continuum emission as previously noted by Liu et al. (2015). The dust continuum emission is believed to trace the total gas column density well, although it is weighted by the dust temperature. If DCN experiences the same fractionation processes as HDCS, both species should show similar abundance ratios in the observed region. But in the very warm dense cores of positions 4 and 6, we found 3–5 times higher values of the DCN/HDCS ratio than in other positions, which implies that they result from the different fractionation processes between two species.

The high DCN abundance in these warm dense cores can probably result from two mechanisms. The first is the evaporation of highly deuterated species from grain mantles, produced previously in the cold gas phase before depletion. There could also be further fractionation processes on the grain surface. Methanol emission detected in these positions (Minh et al. 2016) suggests that the grain mantles are evaporating in the limited central areas associated with star formations. The DCN emission is, however, widespread and not concentrated particularly in the star-forming core regions. In addition, if the DCN abundance mainly results from grain desorption, both DCN and HDCS may show a similar tendency in abundance ratio. The second mechanism for the DCN enhancement is the deuteration fractionation process through CH_2D^+ in the lukewarm gas, as reviewed in Section 1. The DCN emission is widespread similarly to the emission found, for instance, in Busquet et al. (2017), which was interpreted as resulted from the lukewarm chemistry. Considering the physical condition of these positions, the large abundance of DCN must be related to the increased density and temperature relative to other positions, and the lukewarm chemistry may efficiently enhance the deuterium fractionation of HCN in these regions. Then the DCN may have formed in the "later" phase of star formation in the dense gas near newly formed stars.

5. Summary

We investigated the emission from two deuterated species, DCN and HDCS, in a massive star-forming region, G33.92 +0.11, observed at sub-arcsecond angular resolution (0.″6–0.″8) using ALMA. The sub-clumps in this region show complex chemical features resulting from massive star formation activities where gas is still accreting from ambient clouds. HDCS is suggested to mainly form in cold gas through the typical deuterium fractionation reactions, including H_2D^+, and it traces the cold pre-collapse gas before the star formation. The large abundance of HDCS in position 1 suggests that there still exists a large abundance of cold gas in the present active star-forming site. The high value of the HDCS/H_2CS ratio in position 3 suggests that cold dense pristine gas probably existed before the overall cloud collapse. DCN shows a good correlation with the dust continuum emission. Large values of the DCN/HDCS abundance ratio were found toward positions 4 and 6 associated with the region where stars have already formed. The DCN enhancement in these positions may be influenced by the post-stage activities of star formation, since this species can be fractionated efficiently in the lukewarm gas-phase led by the reaction with CH_2D^+.

J.H. thanks the support from the National Natural Science Foundation of China (U1631237), Yunnan Province of China (No.2017HC018) and the Chinese Academy of Sciences (CAS), through a grant to the CAS South America Center for Astronomy (CASSACA) in Santiago, Chile.

This paper makes use of the following ALMA data: ADS/JAO.ALMA#2012.1.00387.S. ALMA is a partnership of ESO (representing its member states), NSF (USA) and NINS (Japan), together with NRC (Canada), MOST and ASIAA (Taiwan), and KASI (Republic of Korea), in cooperation with the Republic of Chile. The Joint ALMA Observatory is operated by ESO, AUI/NRAO and NAOJ.

Table 3
Abundances of the Observed Species

Pos.[a]	DCN (cm^{-2}) [%]	HDCS (cm^{-2}) [%]	$H_2C^{34}S$ (cm^{-2}) [%]	H_2[b] (cm^{-2})	$\frac{DCN}{H_2}$	$\frac{H_2CS}{H_2}$[c]	$\frac{HDCS}{H_2CS}$[c]	$\frac{DCN}{HDCS}$
1 (A5)	0.8(13) [29]	2.9(13) [32]	3.5(13) [25]	4.0(22)	2.0(−10)	1.8(−8)	0.028	0.40
2 (A5)	0.3(13) [30]	0.8(13) [47]	3.0(13) [29]	2.6(22)	1.2(−10)	2.3(−8)	0.014	0.32
3	0.9(13) [29]	2.5(13) [31]	1.1(13) [29]	4.2(22)	2.1(−10)	0.5(−8)	0.12	0.35
4 (A1)	1.3(13) [29]	1.0(13) [40]	3.6(13) [25]	6.6(22)	2.0(−10)	1.1(−8)	0.013	1.4
5 (A9)	0.7(13) [29]	1.4(13) [39]	3.0(13) [30]	3.6(22)	1.9(−10)	1.7(−8)	0.023	0.49
6 (A2)	2.9(13) [29]	1.2(13) [36]	2.5(13) [72]	9.0(22)	3.2(−10)	0.6(−8)	0.025	2.4

Notes. "$x(y)$" in numbers means "$x \times 10^y$." Numbers in brackets at the right side of column density values are the estimated uncertainties of the column density in percentage (Section 3).
[a] Positions are shown in the continuum map of Figure 1 with red circles.
[b] Derived from the dust continuum intensity (Section 3).
[c] H_2CS values were calculated from $H_2C^{34}S$ using the isotope ratio $CS/C^{34}S = 20$ (Chin et al. 1996) as explained in Section 3.

ORCID iDs

Young Chol Minh https://orcid.org/0000-0003-1742-0119
Jinhua He https://orcid.org/0000-0002-3938-4393

References

Aikawa, Y., Ohashi, N., Imtsuka, S., et al. 2001, ApJ, 552, 639
Bacmann, A., Lefloch, B., Ceccarelli, C., et al. 2003, ApJL, 585, L55
Belloche, A., Müller, H. S. P., Garrod, R. T., et al. 2016, A&A, 587, A91
Busquet, G., Fontani, F., Viti, S., et al. 2017, A&A, 604, A20
Caselli, P., Walmsley, C. M., Tafalla, M., et al. 1999, ApJL, 523, L165
Ceccarelli, C., Caselli, P., Herbst, E., et al. 2007, in Protostars and Planets V, ed. B. Reipurth, D. Jewitt, & K. Keil (Tucson, AZ: Univ. Arizona Press), 47
Ceccarelli, C., Loinard, L., Castets, A., et al. 2001, A&A, 372, 998
Chin, Y.-N., Henkel, C., Whiteoak, J. B., et al. 1996, A&A, 305, 960
Daniel, F., Cernicharo, J., Roueff, E., et al. 2007, ApJ, 667, 980
Das, A., Sahu, D., Majumdar, L., & Chakrabarti, S. K. 2016, MNRAS, 455, 540
Emprechtinger, M., Caselli, P., Volgenau, N. H., et al. 2009, A&A, 493, 89
Fish, V. L., Reid, M. J., Wilner, D. J., & Churchwell, E. 2003, ApJ, 587, 701
Fontani, F., Busquet, G., Palau, A., et al. 2015, A&A, 575, A87
Fontani, F., Palau, A., Caselli, P., et al. 2011, A&A, 529, L7
Gerlich, D., Herbst, E., & Roueff, E. 2002, P&SS, 50, 1275
Gerner, T., Shirley, Y. L., H. Beuther, H., et al. 2015, A&A, 579, A80
Ginard, D., González-García, M., Fuente, A., et al. 2012, A&A, 543, A27
Hatchell, J., Thompson, M. A., Millar, T. J., & Macdonald, G. H. 1998, A&A, 338, 713
Herbst, E., & van Dishoeck, E. F. 2009, ARA&A, 47, 427
Irvine, W. M., Goldsmith, P. F., & Hjalmarson, Å. 1987, in Interstellar Processes, 134 ed. D. J. Hollenbach & H. A. Thronson, Jr. (Dordrecht: Reidel), 561
Jefferts, K. B., Penzias, A. A., & Wilson, R. W. 1973, ApJL, 179, L57
Leurini, S., Rolffs, R., Thorwirth, S., et al. 2006, A&A, 454, L47
Linsky, J. L., Brown, A., Gayley, K., et al. 1993, ApJ, 402, 694
Lis, D. C., Gerin, M., Phillips, T. G., & Motte, F. 2002, A&A, 569, 322
Liu, H. B., Galvań-Madrid, R., Jimeńez-Serra, I., et al. 2015, ApJ, 804, 37
Liu, H. B., Jiménez-Serra, I., Ho, P. T. P., et al. 2012, ApJ, 756, 10
Loinard, L., Castets, A., Ceccarelli, C., et al. 2000, A&A, 359, 1169
Loinard, L., Castets, A., Ceccarelli, C., et al. 2001, ApJL, 552, L163
López-Sepulcre, A., Taquet, V., Sánchez-Monge, Á, et al. 2013, A&A, 556, A62
Marcelino, N., Cernicharo, J., Roueff, E., et al. 2005, ApJ, 620, 308
Meier, R., Owen, T. C., Jewitt, D. C., et al. 1998, Sci, 279, 1707
Minh, Y. C., Liu, H. B., & Galvań-Madrid, R. 2016, ApJ, 824, 99
Minowa, H., Satake, M., Hirota, T., et al. 1997, ApJL, 491, L63
Oliveira, C. M., Hébrard, G., Howk, J. C., et al. 2003, ApJ, 587, 235
Osamura, Y., Roberts, H., & Herbst, E. 2004, A&A, 421, 1101
Parise, B., Leurini, S., Schilke, P., et al. 2009, A&A, 508, 737
Pillai, T., Wyrowski, F., Hatchell, J., et al. 2007, A&A, 467, 207
Reipurth, B., & Yan, C.-H. 2008, in ASP Conf. Ser. 402, Handbook of Star-forming Regions, Vol. I, ed. B. Reipurth (San Francisco, CA: ASP), 869
Ren, Z., Wu, Y., Zhu, M., et al. 2012, MNRAS, 422, 1098
Roberts, H., Fuller, G. A., Millar, T. J., et al. 2002, A&A, 381, 1026
Roberts, H., Herbst, E., & Millar, T. J. 2002, MNRAS, 336, 283
Roberts, H., & Millar, T. J. 2000, A&A, 361, 388
Rodgers, S., & Millar, T. 1996, MNRAS, 280, 1046
Roueff, E., & Gerin, M. 2003, SSRv, 106, 61
Roueff, E., Gerin, M., Lis, D. C., et al. 2013, JPCA, 117, 9959
Roueff, E., Parise, B., & Herbst, E. 2007, A&A, 464, 245
Tan, J. C., Beltrán, M. T., Caselli, P., et al. 2014, in Protostars and Planets VI, ed. H. Beuther et al. (Tucson, AZ: Univ. Arizona Press), 149
Tiné, S., Roueff, E., Falgarone, E., et al. 2000, A&A, 356, 1039
Turner, B. E. 2001, ApJS, 136, 579
van der Tak, F. F. S., Boonman, A. M. S., Braakman, R., & van Dishoeck, E. F. 2003, A&A, 412, 133
van Dishoeck, E. F., Blake, G. A., Jansen, D. J., & Groesbeck, T. D. 1995, ApJ, 447, 760
Watt, S., & Mundy, L. G. 1999, ApJS, 125, 143
Willacy, K. 2007, ApJ, 660, 441
Wilson, T. L., & Rood, R. T. 1994, ARA&A, 32, 191
Zinchenko, I., Liu, S.-Y., Su, Y.-N., et al. 2012, ApJ, 755, 177
Zinnecker, H., & Yorke, H. W. 2007, ARA&A, 45, 481